Semiclassical dynamics simulations of charge transport in stacked -systems

Felix Plasser and Hans Lischka

Citation: The Journal of Chemical Physics **134**, 034309 (2011); doi: 10.1063/1.3526697
View online: http://dx.doi.org/10.1063/1.3526697
View Table of Contents: http://scitation.aip.org/content/aip/journal/jcp/134/3?ver=pdfcov
Published by the AIP Publishing

Semiclassical dynamics simulations of charge transport in stacked π-systems

Felix Plasser[a] and Hans Lischka[b]
Institute for Theoretical Chemistry – University of Vienna, Waehringerstrasse 17, A 1090 Vienna, Austria

(Received 18 August 2010; accepted 23 November 2010; published online 20 January 2011)

Charge transfer processes within stacked π-systems were examined for the stacked ethylene dimer radical cation with inclusion of a bridge containing up to three formaldehyde molecules. The electronic structure was treated at the complete active space self-consistent field and multireference configuration interaction levels. Nonadiabatic interactions between electronic and nuclear degrees of freedom were included through semiclassical surface hopping dynamics. The processes were analyzed according to fragment charge differences. Static calculations explored the dependence of the electronic coupling and on-site energies on varying geometric parameters and on the inclusion of a bridge. The dynamics simulations gave the possibility for directly observing complex charge transfer and diabatic trapping events. © *2011 American Institute of Physics*. [doi:10.1063/1.3526697]

I. INTRODUCTION

The dynamics of charge migration in molecular systems have attracted widespread interest. For example, the transport of electron holes has been studied in DNA because of its relation to oxidative damage[1] but also because DNA might provide interesting prototypes for nanoelectronics.[2] Charge dynamics plays an important role also in organic electronics.[3] Therefore, it is highly desirable to get more detailed physical insight into this important class of processes. Based on computational studies and charge injection experiments it has been proposed that a coherent superexchange mechanism with no or little[4] involvement of the bridge is involved between stacked nucleobases if the bridge length is three bases or less whereas charge transfer over longer distances should occur through an incoherent hopping mechanism.[5]

The general features of a system governed by a defect localized on two interacting fragments are shown in Scheme 1. The on-site energies of the initial and final charge-localized (diabatic) states H_{ii}^{diab} and H_{ff}^{diab} are represented as displaced parabolas along the reaction coordinate ξ. The reorganization energy λ, is the energy needed for moving the system from one diabatic minimum to the other while maintaining the initial diabatic character (in a symmetric system this is equivalent to the vertical excitation at one minimum). The interaction between the two diabatic states is given by the coupling matrix element H_{if}^{diab}. Diagonalization of the two-dimensional **H** matrix yields the adiabatic energies E_1^{ad} and E_2^{ad} of the ground and first excited electronic states. In the case of strong interaction [$H_{if}^{\text{diab}} > \lambda/2$; Scheme 1(a)], E_1^{ad} as a function of ξ possesses one symmetric minimum where the eigenfunction of **H** is delocalized. If the interaction is weaker [$H_{if}^{\text{diab}} < \lambda/2$; Scheme 1(b)], two minima are present where the charge is localized on either side. If the coupling is strong, the states are well separated and adiabatic dynamics on the ground state occurs. In the weak coupling limit, on the other hand, the diabatic character is nearly always preserved and the interaction between the states can be treated as a small perturbation. In this case, the rate of transfer can be described by the semiclassical Marcus–Levich–Hush (MLH) equation.[6–9] A more detailed explanation of this relation and its connection to our dynamics simulations will be given in Sec. II. Extensions of the MLH equation include corrections for quantum effects for selected normal modes, but these are usually important only for low temperatures (below 100 K) or in the Marcus-inverted region.[7,8,10] No simple approach exists in the region of $H_{if}^{\text{diab}} \approx \lambda/2$.[10] This region which may be treated by explicit nonadiabatic dynamics simulations is the focus of this work.

In the usual approach, the parameters are estimated from static calculations and then inserted into the MLH equation.[11] One difficulty in this procedure is the fact that the description of open-shell cationic systems is highly challenging and there are problems with many of the standard methods in quantum chemistry. A major problem is an artificial localization of the hole, which means that the wave function obtained does not represent the true adiabatic ground state of the system. This has been observed in the case of polycyclic organic radical cations for unrestricted Hartree–Fock,[12] as well as for single reference configuration interaction and second-order Møller–Plesset perturbation theory.[13] Unrestricted B3LYP gave the opposite trend of overstabilizing the charge-delocalized structures.[12] Several indirect approaches have been developed in an attempt to overcome these deficiencies. To avoid the problems of describing the charged system directly, calculations have been carried out in the neutral systems and one-electron Koopmans'-type considerations were used for calculating the CT parameters.[14–16] Other ideas involve spin-flipping to give equal orbital occupations or unrestricted Hartree–Fock to represent diabatic states.[16] Diabatization may be induced through constrained density functional theory as well.[11,17] In spite of the fact that all these ways to approach the problem give good results in

[a]Electronic mail: felix.plasser@univie.ac.at.
[b]Electronic mail: hans.lischka@univie.ac.at.

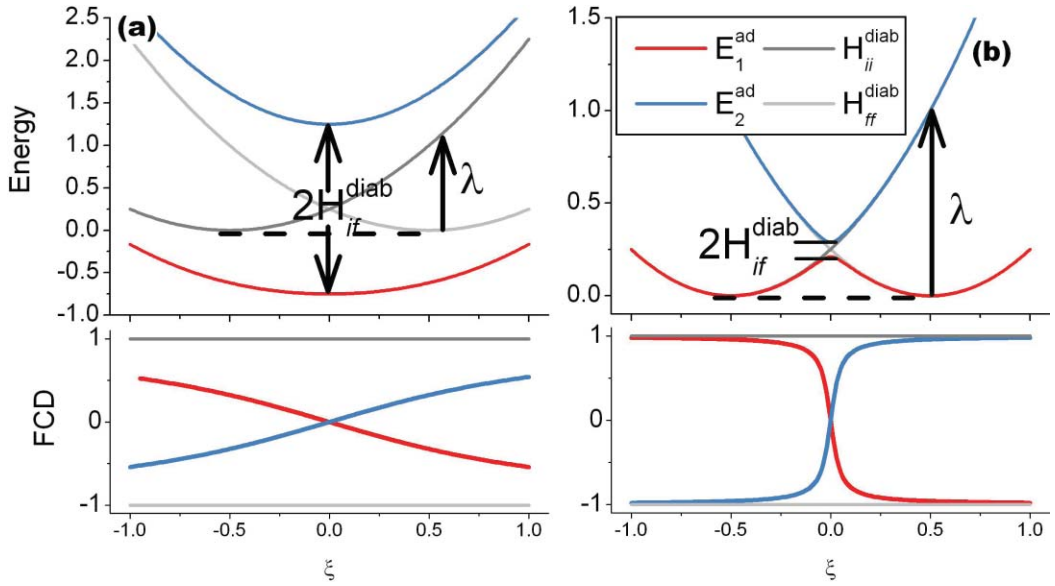

SCHEME 1. Model potential energy curves and fragment charge differences (FCD) plotted against the reaction coordinate ξ for a defect distributed over two interacting fragments for the cases of (a) strong and (b) weak coupling.

some cases, they suffer from the fact that *ad hoc* assumptions are needed. Recent investigations show that there is reasonable agreement but that Koopmans' theorem overestimates the energy gaps.[18] Another problem is the static approach relying on the assumptions made in the derivation of the MLH equation, i.e., validity of the weak coupling limit, constant coupling, and a fixed form of the potential. Force-field molecular dynamics in connection with semiempirical methods have been performed to efficiently sample the large conformational spaces of the DNA structure and to calculate the electronic coupling elements,[4,15] but these methods suffer from the fact that they do not couple nuclear and electronic dynamics in a consistent way. Note that models from solid state physics have been used as well, in particular for DNA. Then molecular motion and aperiodicity can cause difficulties.[2,19]

In this work, nonadiabatic dynamics simulations are used to directly couple the nuclear and electronic dynamics. The ethylene dimer radical cation with insertion of a bridge of up to three formaldehyde molecules (Scheme 2) is examined with the goal to model the principal features of charge migration in DNA. The reason for this choice is that this system is well suited for studying charge-hopping between π-systems and is also small enough to allow accurate investigation of the energy surfaces and extended dynamics simulations. The complex offers the possibility to study the major physical effects through changes in CC bond length alternation and intermolecular distance.

The use of multireference *ab initio* electronic structure computations is coupled to semiclassical dynamics. This type of approach has been used very successfully in the field of photodynamics (see, e.g., Ref. 20). But to our knowledge, *ab initio* direct descriptions of charged systems[13,18,21] and semiclassical dynamics in this context[12,22] have been performed only rarely. We perform state-averaged complete active space self-consistent-field computations (SA-CASSCF), which allow for a high-level explicit treatment of the quasi-degeneracies of the two charged states involved. Dynamical electron correlation is added through the multireference configuration interaction approach (MR-CI). The nonadiabatic coupling between electronic and nuclear degrees of freedom is directly included through semiclassical surface hopping dynamics.[23] In this way it is possible to treat the electronic structure and nonadiabatic effects simultaneously at a high level, including all internal degrees of freedom and the whole spectrum of coupling strengths between the adiabatic and nonadiabatic limits can be treated.

II. METHODS

In this section, we first briefly introduce the surface hopping method and discuss its applicability to defect dynamics. Then we elucidate how deeper physical insight may be gained

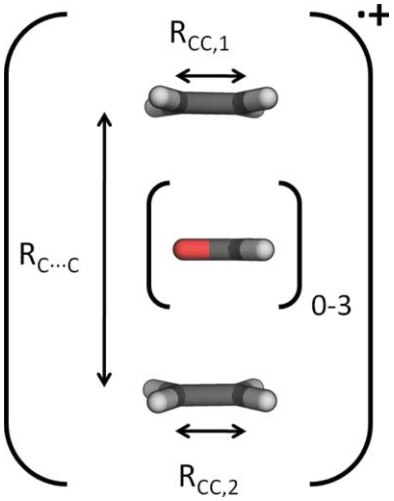

SCHEME 2. Molecular structure of $[Et.–(FA)_n–Et.]^+$ ($n = 0$–3) complexes studied in this work and definition of internal coordinates.

from this dynamics and how the results may be compared with the physical models in use.

Within the surface hopping method, nuclear motion is treated by classical dynamics coupled to forces coming from an electronic structure calculation. Several electronic states are considered simultaneously, each one associated with a complex amplitude A_k. The electronic Schrödinger equation (considering adiabatic states) is propagated in the following way:

$$\dot{A}_k(t) = -\sum_{l \neq k} A_l(t) e^{i\gamma_{kl}} \dot{\mathrm{R}} \cdot \mathrm{h}_{kl}, \tag{1}$$

$$\gamma_{kl}(t) = \frac{1}{\hbar} \int_0^t \left(E_k^{\mathrm{ad}}(\mathrm{R}(t)) - E_l^{\mathrm{ad}}(\mathrm{R}(t)) \right) dt, \tag{2}$$

$$h_{kl}^{(j)}(\mathrm{R}) = \left\langle \Psi_k^{\mathrm{ad}} \middle| \frac{\partial}{\partial R_j} \middle| \Psi_l^{\mathrm{ad}} \right\rangle. \tag{3}$$

The adiabatic electronic energies E_k^{ad} and the nonadiabatic couplings $\mathbf{h}_{kl}$ are needed for propagating the amplitudes A_k. The electronic energy gradient of the "active" or "current" state is needed for propagating the geometry $\mathbf{R}$. E_k^{ad}, $\mathbf{h}_{kl}$, and the gradient of the "active" state are computed with an appropriate electronic structure method. The essence of surface hopping is that the system follows a classical trajectory on the respective "active" state surface, while the electronic wave packet evolves according to Eq. (1). In the case of population transfer, the "active" state is changed in a stochastic manner. With this approach, the time dependent quantum mechanical coupling between nuclear and electronic degrees of freedom can be modeled in a framework of independent trajectories. For more information, see Refs. 23 and 24.

For a physical interpretation it is helpful to consider the dynamics in a two state model (cf. Refs. 8 and 14).

$$\begin{pmatrix} \Psi_1^{\mathrm{ad}} \\ \Psi_2^{\mathrm{ad}} \end{pmatrix} = U \begin{pmatrix} \Psi_i^{\mathrm{diab}} \\ \Psi_f^{\mathrm{diab}} \end{pmatrix} \tag{4}$$

$$U = \begin{pmatrix} \cos(\eta) & -\sin(\eta) \\ \sin(\eta) & \cos(\eta) \end{pmatrix} \tag{5}$$

The adiabatic ground state Ψ_1^{ad} and first excited state Ψ_2^{ad} are formed as linear combinations of two charge localized "diabatic" states Ψ_i^{diab} and Ψ_f^{diab}. The diabatic states are chosen such that Ψ_i^{diab} has the charge on the "initial" fragment and Ψ_f^{diab} on the "final" fragment. Such a construction based on physical observables will usually diminish the nonadiabatic couplings between these states and "diabaticity" should be present in this sense.[11,25] In principle, all quantities of Eqs. (4) and (5) are geometry dependent but the first approximation is to view the diabatic states as independent on molecular geometry which would, of course, make the nonadiabatic couplings vanish completely.[26] It is generally not possible to construct a set of strictly diabatic states starting from adiabatic states.[11] Therefore, a large number of approximate diabatization schemes exist.[11] In this work, the fragment charge difference (FCD) method [where Δq_i denotes the charge difference (in atomic units) between the two fragments in state i] is used for the characterization of the charge-localized states.[14,16] Under the assumption of (4), i.e., that there are just two orthogonal diabatic states involved, the following relation between the mixing angle η and the FCDs of the ground ($i = 0$) and excited ($i = 1$) state is obtained:[14]

$$-\Delta q_1(\mathbf{R}) = \Delta q_0(\mathbf{R}) = \cos(2\eta(\mathbf{R})). \tag{6}$$

Analogously to (4), the Hamiltonian may be transformed between the adiabatic and diabatic basis.

$$\begin{pmatrix} E_1^{\mathrm{ad}} & 0 \\ 0 & E_2^{\mathrm{ad}} \end{pmatrix} = U^{\mathrm{T}} \begin{pmatrix} H_{ii}^{\mathrm{diab}} & H_{if}^{\mathrm{diab}} \\ H_{if}^{\mathrm{diab}} & H_{ff}^{\mathrm{diab}} \end{pmatrix} U. \tag{7}$$

All quantities of Eq. (7) are geometry dependent. However, in analogy to the Condon approximation it is often assumed that the interaction matrix element H_{if}^{diab} is constant for fixed intermolecular distance.[10] It can then be computed as half of the energy gap at resonance conditions.[16] Note that under this assumption no conical intersection between the adiabatic states is expected to be present, as the gap may never go below $2\ H_{if}^{\mathrm{diab}}$. The geometry dependence of the on-site energies H_{ii}^{diab} and H_{ff}^{diab} can be approximated by parabolas around the respective minima (Scheme 1).[10]

Our surface hopping simulations include two adiabatic states, which can be thought of as linear combinations of the charge localized diabatic states. An adiabatic trajectory moving from one minimum (where $\eta = 0$) to the other minimum ($\eta = \pi/2$) would necessarily transfer the charge. Physically, such a charge transfer corresponds to electron tunneling. In the case of small electronic coupling H_{if}^{diab} (typically because of large spatial separation), the electron tunneling speed may be on the same order or even much slower than nuclear motion. It is therefore necessary to integrate the electronic Schrödinger equation along with the nuclear motion. Surface hopping, as described earlier, is an efficient method for such nonadiabatic treatment. Electron tunneling occurs in connection with an adiabatic nuclear dynamics [Scheme 3(a)], whereas an avoided tunneling event, i.e., diabatic trapping, is represented through two consecutive surface hops [cf. Scheme 3(b) and Ref. 22].

To get better understanding of these events it is helpful to reformulate the surface hopping equations in the two-state model. If, as described earlier, the nonadiabatic coupling between the diabatic states vanishes, the nonadiabatic coupling between the adiabatic states corresponds to the change in the mixing angle η [see also Eqs. (2.18)–(2.22) of Ref. 27].

$$h_{12}^{(i)}(\mathbf{R}) = \frac{\partial \eta(\mathbf{R})}{\partial R_i}. \tag{8}$$

Then the amplitude propagation [cf. Eq. (1)] may be rewritten

$$-\frac{\dot{A}_1(t)}{A_2(t)} = e^{i\gamma_{12}(t)} \frac{\partial \eta}{\partial t}(t). \tag{9}$$

In this formulation it can be seen that a quick change in η (relative to the speed of change in γ_{12}) is compensated by a corresponding change in the A_i's leading to no change in the diabatic character of the total time dependent electronic wave function. A charge transfer only occurs if the change in the

relative phase factor γ_{12} (which is proportional to the energy gap) is faster than the change in η.

For the analysis of the dynamics, kinetic equations as derived by Brunschwig *et al.*[8] were considered. One starts with the Eyring equation

$$k_{\mathrm{CT}} = \kappa_{\mathrm{el}} \nu e^{-\frac{\Delta G^{\neq}}{kT}}, \tag{10}$$

where κ_{el} is the electronic transmission coefficient, ν is the frequency of the active vibration, and $\Delta G^{\neq}$ is the Gibbs free activation energy. In the next step, under the assumption that the diabatic coupling is negligible, $\Delta G^{\neq}$ can be written in terms of the reaction free energy $\Delta_{\mathrm{r}}G$ and the reorganization energy λ as[9]

$$\Delta G^{\neq} = \frac{\lambda}{4}\left(1 + \frac{\Delta_r G}{\lambda}\right)^2. \tag{11}$$

In the case of a symmetric reaction potential, i.e., $\Delta_{\mathrm{r}}G = 0$, Eq. (11) reduces to

$$\Delta G^{\neq} = \frac{\lambda}{4}. \tag{12}$$

To obtain κ_{el}, one starts from the Landau[28]–Zener[29] probability

$$P_{12} = 1 - \exp\frac{-4\pi^2\left(H_{if}^{\mathrm{diab}}\right)^2}{h\mathrm{Vs}} \tag{13}$$

of performing a charge transfer (i.e., remaining on the same adiabatic surface) per single passage over the transition state where **V** is the velocity, and **s** the difference in slopes. Eq. (13) may be rewritten as

$$P_{12} = 1 - \exp\left(\frac{-\left(H_{if}^{\mathrm{diab}}\right)^2}{h\nu}\sqrt{\frac{\pi^3}{\lambda kT}}\right) \tag{14}$$

to obtain a form with more readily available quantities.[8,30]

P_{12} is the probability of a CT for a single passage over the transition state. If this CT is avoided the system has switched from the ground to the excited state. The excited state may relax through an additional *TS passage* leading to a recrossing and diabatic trapping situation. Alternatively, the system may switch to the CT product state after one or more *TS passages* in the excited state. Therefore, it may be seen that the probability κ_{el} of CT per *global TS* crossing event is higher than per single passage. Assuming that the events are independent of each other (i.e., there is no electronic coherence) and that the transition probability is the same for every TS passage, it can be written as (see also Refs. 8 and 12):

$$\begin{aligned}\kappa_{\mathrm{el}} &= P_{12} + (1 - P_{12})P_{12}(1 - P_{12}) \\ &\quad + (1 - P_{12})P_{12}^3(1 - P_{12}) + \cdots \\ &= \frac{2P_{12}}{1 + P_{12}},\end{aligned} \tag{15}$$

where the first two terms in the sum correspond to the respective processes of Scheme 3(a) and 3(c), and the remaining terms correspond to higher order events. As shown in Ref. 8, the quantities derived earlier can be combined to form the well-known Marcus–Levich–Hush equation for the charge transfer reaction constant. In this work, we will specifically focus on the electronic transmission coefficient κ_{el} and the related quantity P_{12}. These quantities are evaluated as relations between the following four elementary processes (two geometrical and two charge-transfer cases):

1. *Transition state (TS) passage*: Single passage over the TS with a sign change in the generalized reaction coordinate ξ. This coordinate is identified with the FCD (always taken for the same adiabatic state, e.g., D_0) as function of the nuclear coordinates, i.e., $\Delta q_0 = \Delta q_0(\mathbf{R})$.
2. *TS global*: This process starts in the ground state with the charge on one side and describes the overall process of reaching the TS and finally arriving in one of the potential wells of the ground state again (crossing or returning).
3. *Active charge transfer (CT)*: This is a charge transfer event in the "active" state related to a single *TS passage*. It occurs for an adiabatic process (if there is no change of state).
4. *Real CT*: This is a process related to *TS global*, which starts with the charge in the ground state on one side and finally ends with the charge in the ground state on the other side (in between several *TS passages* with or without *active CTs* may have happened).

In Scheme 3, we illustrate these processes for the hierarchy of *global TS* events arranged according to the number of *TS passages* taking place. The simplest example [Scheme 3(a)] is the adiabatic charge transfer moving from one minimum to the other, always remaining on the adiabatic ground state. The ground state FCD curve (full black line) illustrates the *TS passage* with the required sign change in the charge as discussed in item 1 above. The *active CT* is represented by the sign change of the red circles (FCD in the active state). The process is also connected with a *real CT*, i.e., a net charge transfer from one minimum to the other. The energy gap, presented on top of the FCD plot, is reduced to $2\ H_{if}^{\mathrm{diab}}$ at the avoided crossing. The diabatic trapping situation (two *TS passages*) in Scheme 3(b) starts in the left minimum. Along with the first *TS passage* (first sign change of the black FCD curve), there is a surface hopping to the excited state (a change in the adiabatic state that preserves the diabatic character) and the charge remains on the same fragment (no sign change of the FCD, red circles, and therefore, no *active CT*). On the second *TS passage*, the system hops back to the ground state into the original energy minimum. During this whole process, there is no *CT* (*real* or *active*). The next event [Scheme 3(c)] contains three *TS passages*. It starts like Scheme 3(b) but the system remains in the excited state during the second *TS passage* and the charge is transferred in the excited state (sign change of the FCD, red circles, active state is in D_1). A third *TS passage* with a hopping to the ground state brings the system diabatically to the right minimum, completing the *real CT*. The following event in this hierarchy (not shown in Scheme 3) would contain four *TS passages*, the first one with a hop to the excited state followed by two *active CTs* in the excited state and a hop to the ground state on the fourth *passage* followed by a relaxation to the initial minimum. There would be no net charge transfer and therefore no *real CT*.

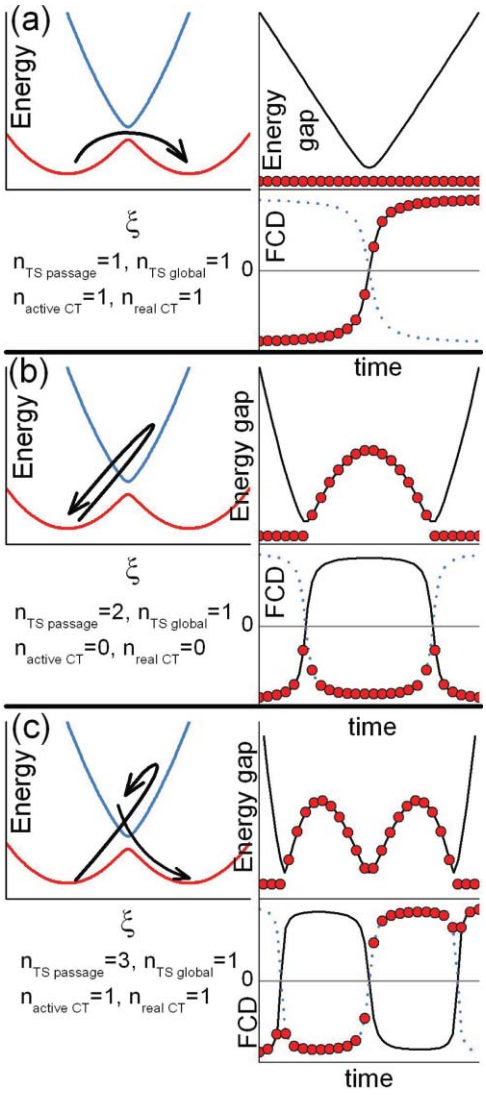

SCHEME 3. Schematic depiction of global processes around the crossing region. Left plots show the processes with respect to the reaction coordinate ξ (blue: excited state, red: ground state). Right plots show the corresponding time evolution of the energy gap and fragment charge difference (FCD) (blue dots: excited state, black line: ground state, red circles: "active" state). (a) Represents an adiabatic charge transfer; (b) a diabatic trapping situation; and (c) a higher order process, finally leading to a charge transfer.

The four processes defined earlier (*TS passage*, *TS global*, *active CT*, and *real CT*) were used to analyze the charge transfer and trapping events during the dynamics. The microscopic P_{12} probability corresponds to the fraction of *TS passages* leading to *active CTs*. It is, therefore, obtained as the ratio between the numbers of these two processes counted during the dynamics:

$$P_{12} = \frac{\mathrm{n}_{activeCT}}{\mathrm{n}_{TSpassage}}. \tag{16}$$

The macroscopic transmission coefficient κ_{el}

$$\kappa_{el} = \frac{\mathrm{n}_{realCT}}{\mathrm{n}_{TSglobal}} \tag{17}$$

is computed as the ratio between the number of *TS global* and *real CT* events. To compare theory and results, we may check if relation (15) holds with respect to these two quantities.

III. COMPUTATIONAL DETAILS

A symmetric face-to-face arrangement of the ethylene dimer radical cation $[\mathrm{Et.–Et.}]^+$ and of this system with 1–3 formaldehyde molecules inserted $[\mathrm{Et.–(FA)}_n\mathrm{–Et.}]^+$ ($n = 1$–3) with parallel molecular planes was constructed (Scheme 2). Computations on the $[\mathrm{Et.–Et.}]^+$ complex were generally performed with C_{2v} symmetry with the z-axis going through the molecular planes, and the y-axis parallel to the molecular CC axes (note that in the case of equal CC bond lengths the complex actually possesses D_{2h} symmetry). The main parameters of interest were the *inter*molecular C · · · C distances $R_{\mathrm{C}\cdots\mathrm{C}}$ (kept at equal values for both sides) and the bond length alternation coordinate ΔR, which was formed as a difference between the two *intra*molecular CC distances

$$\Delta R = R_{CC,1} - R_{CC,2}. \tag{18}$$

Up to three formaldehyde molecules were inserted between the two ethylene molecules. The maximum symmetry of C_{2v} was chosen for the symmetric geometry, i.e., $\Delta R = 0$ (z-axis parallel to the molecular axes and the x-axis perpendicular to the molecular planes). In the displaced case, i.e., $\Delta R \neq 0$, C_{s} symmetry was used (y-axis parallel to the molecular axes and the x-axis perpendicular to the molecular planes).

State-averaged complete active space self-consistent-field (CASSCF) computations were performed for the $[\mathrm{Et.–Et.}]^+$ and $[\mathrm{Et.–(FA)}_n\mathrm{–Et.}]^+$ ($n = 1$–3) complexes with three electrons in the four orbitals formed from the two π and two π^* orbitals of the ethylene molecules with state averaging over the doublet ground and first excited states (SA(2)-CASSCF(3/4)). State averaging was performed to get a balanced description of the two states that were obtained by removing an electron from the respective π orbital. It has been noted that this procedure can overcome spurious charge localization which many other methods suffer from.[13] This corresponded to two A_1 states in $[\mathrm{Et.–Et.}]^+$ (C_{2v}), one B_1 and one A_1 state for the symmetric (C_{2v}), and two A′ states for the displaced (C_{s}) $[\mathrm{Et.–(FA)}_n\mathrm{–Et.}]^+$ ($n = 1$–3) complexes.

Dynamic electron correlation was taken into account through multireference configuration interaction with single and double excitations (MR-CISD). Based on previous experience gained with MRCI calculations on π systems,[31] appropriate reference spaces have been chosen. Unless specified differently, the reference space was identical to the CAS(3/4) of the preceding CASSCF calculation. To allow for a consistent treatment of different symmetry groups, no generalized interacting space restrictions were imposed and all irreducible representations of the respective symmetry group were allowed as reference symmetries. Higher-order excitations[32,33] were taken into account in single point calculations by means of corrections proposed by Pople *et al.*[34] (+P). The 6–31G*[35] and 6–311+G*[36] basis sets were used. Fragment charge differences were obtained by summing over Mulliken charges. The electronic structure computations were performed with the COLUMBUS[37] program package using electronic integrals computed with DALTON.[38]

Optimizations of $[\mathrm{Et.–Et.}]^+$ were performed in the C_{2v} subspace, thus retaining a face-to-face arrangement. Three distances 3.0, 5.0, and 7.0 Å were chosen for $R_{\mathrm{C}\cdots\mathrm{C}}$ in

order to represent the cases of strong, intermediate, and weak coupling. For these structures, the intramolecular coordinates were optimized for the D_{2h} geometry (with $\Delta R = 0$) as well as the full minimum in C_{2v}. For the [Et.–(FA)$_n$–Et.]$^+$ (n = 1–3) complexes an intermolecular distance of 3.5 Å between adjacent molecules was chosen and a face-to-face arrangement was selected. For $n = 1$ and 2, intramolecular coordinates were optimized for the symmetric C_{2v} structure and the C_s minima. For $n = 3$, the stack was constructed without further optimization.

Nonadiabatic surface hopping dynamics simulations with Tully's fewest-switches algorithm[23] were carried out with the NEWTON-X[39,40] package. An empirical decoherence correction as described in Ref. 41 with a decay parameter of 0.1 Hartree was included to permit a more realistic treatment of recrossings through the transition region. Electronic energies, gradients, and nonadiabatic couplings[33,42] were computed at the SA(2)-CASSCF(3/4) level with the 6–311+G* basis set for [Et.-Et.]$^+$ and 6–31G*[43] for [Et.–FA–Et.]$^+$. A time step 0.5 fs was chosen. Fifty trajectories with a simulation time of 1 ps each were computed for each of the complexes. The initial conditions were chosen from a Wigner distribution of the harmonic vibrational ground state of the charge localized minimum as described in Ref. 39. To maintain a face-to-face configuration with maximal π-stacking, a restraining potential was applied to restrict relative motion of the molecules in the [Et.–Et.]$^+$ and [Et.–FA–Et.]$^+$ complexes. A harmonic potential in terms of all six, respectively 12, intermolecular normal coordinates with respect to displacement from the reference geometry was added using a spring constant of 0.5 a.u.

An automated dynamics analysis was performed to obtain P_{12} and κ_{el} [Eqs. (16) and (17)]. In the discussion, the following quantities will be used: Δq_0 for the FCD of the adiabatic ground state and Δq_{act} for the FCD of the active state of the Surface Hopping dynamics. In the analysis, a charge delocalization threshold $\alpha = 0.5$ a.u. and a relaxation time $\tau = 3$ fs are included to eliminate spurious results related to the stochastic nature of the dynamics. A *TS passage* was defined to occur if initially the condition $\Delta q_0 < -\alpha$ ($>\alpha$) held for a period of time of at least τ and then $\Delta q_0 > \alpha$ ($<-\alpha$) for at least τ. In an analogous way, an *active CT* was defined to happen if initially $\Delta q_{act} < -\alpha$ ($>\alpha$) for least τ and then $\Delta q_{act} > \alpha$ ($<-\alpha$) for at least τ. A *TS global* event starts if the trajectory is in the ground state and a *TS passage* occurs, it ends if the trajectory is again in the ground state for at least 2τ. It was considered a *real CT* if initially the trajectory was in the ground state and $\Delta q_{act} < -\alpha$ ($>\alpha$) for at least τ and then $\Delta q_{act} > \alpha$ ($<-\alpha$) with the trajectory again in the ground state for at least τ. Note that there are also times where none of the above conditions are fulfilled, e.g., $-\alpha < \Delta q < \alpha$. These parts are ignored in the analysis.

IV. RESULTS AND DISCUSSION

A. Energy surfaces

The geometrical parameters of the optimized complexes are presented in Table I (complete Cartesian geometries and energies are given in S1–S4 of the Supplemental Material[44]). For [Et.–Et.]$^+$, $R_{C\cdots C} = 3.0$ Å, there is one symmetric minimum of D_{2h} symmetry with a delocalized wave function at $R_{CC,1} = R_{CC,2} = 1.375$ Å. In all other cases considered, this symmetric structure was unstable and two minima existed with the charge localized on the longer CC bond. Only a weak dependence of the optimized $R_{CC,1}$ and $R_{CC,2}$ values on the specific complex considered was observed. Moreover, these values were similar to the ones for the isolated ethylene molecule and ethylene radical cation. Only in the [Et.–Et.]$^+$, $R_{C\cdots C} = 5.0$ Å case there is a slight reduction in ΔR (i.e., a trend toward the symmetric minimum) because of stronger coupling present. The geometrical data are not very sensitive to the inclusion of dynamic electron correlation through the MR-CISD method.

The major energetic parameters derived from these calculations (as described in the following paragraph) are collected in Table II. The electronic coupling between the diabatic states H_{if}^{diab} is the decisive quantity for determining the nonadiabatic electron transfer rate.[10,26] Here it is obtained as half the energy gap at the symmetric geometry $\Delta R = 0$.

TABLE I. Structural parameters computed at the SA-CASSCF level of theory (MR-CISD values in parentheses).[a]

		Symm ($\Delta R = 0$)		Relaxed		
Complex	$R_{C\cdots C}$ (Å)	R_{CC} (Å)		$R_{CC,1}$ (Å)	$R_{CC,2}$ (Å)	
Et.[b]				1.338 (1.342)		D_{2h}
(Et.)$^+$[b]					1.403 (1.417)	D_{2h}
[Et.–Et.]$^+$[b,d]	3.00	1.375 (1.378)	D_{2h}	–	–	
[Et.–Et.]$^+$[b]	5.00	1.377 (1.379)	D_{2h}	1.353 (1.345)	1.400 (1.414)	C_{2v}
[Et.–Et.]$^+$[b]	7.00	1.376 (1.378)	D_{2h}	1.343 (1.343)	1.409 (1.414)	C_{2v}
[Et.–FA–Et.]$^+$[c]	7.00	1.376 (1.376)	C_{2v}	1.345 (1.341)	1.407 (1.410)	C_s
[Et.–FA–FA–Et.]$^+$[c]	10.5	1.376	C_{2v}	1.343	1.408	C_s

[a]For definition of coordinates see Scheme 2.
[b]6–311+G* basis set.
[c]6–31G* basis set.
[d]Relaxed structure is symmetric in ΔR.

TABLE II. Energetic parameters of [Et.–(FA)$_n$–Et.]$^+$, (n = 0–3) complexes computed at the SA-CASSCF level of theory (MR-CISD+P values in parentheses).

Complex	$R_{C\cdots C}$ (Å)	H_{if}^{diab} (eV)	Barrier (eV)	λ (eV)
[Et.–Et.]$^+$[a]	3.00	1.1	–	–
[Et.–Et.]$^+$[a]	5.00	7.9E−2 (7.4E−2)	0.006 (0.018)	0.233 (0.314)
[Et.–Et.]$^+$[a]	7.00	4.2E−3 (4.3E−3)	0.042 (0.072)	0.236 (0.281)
[Et.–FA–Et.]$^+$[b]	7.00	3.8E−2 (3.8E−2)	0.028 (0.044)	0.239 (0.294)
[Et.–FA–FA–Et.]$^+$[b]	10.5	2.1E−3	0.059	0.247
[Et.–FA–FA–FA–Et.]$^+$[b]	14.00	1.0E−4	0.058	0.223

[a]6–311+G* basis set.
[b]6–31G* basis set.

The coupling decreases significantly with distance $R_{C\cdots C}$. In contrast, inclusion of an intermediate formaldehyde increases the coupling at constant $R_{C\cdots C}$. For example, at $R_{C\cdots C}$ = 7.0 Å the value is raised by a factor of about 10, reaching almost the coupling of the [Et.–Et.]$^+$ complex at $R_{C\cdots C}$ = 5.0 Å. For these structures, the couplings at the CASSCF level are almost identical to those of the MR-CISD+P benchmarks. The barrier of the adiabatic reaction is the most influential feature for the nuclear part of the dynamics. It was computed as the difference between ground state energy at symmetric and minimum energy geometry. The barrier for [Et.–Et.]$^+$ at $R_{C\cdots C}$ = 7.0 Å is 0.042 eV. At shorter intermolecular distances, the electronic coupling reduces this value. The barrier for [Et.–(FA)$_n$–Et.]$^+$ (n = 2,3) is somewhat larger (0.058 eV), probably because of the additional degrees of freedom present. The reorganization energy λ, computed as the energy gap between D_0 and D_1 at the minimum geometry, is presented as well. For the barrier and reorganization energy, the MR-CISD+P values are somewhat increased compared to the CASSCF values. In the cases of weaker coupling it can be seen that the relation of Eq. (12) is fulfilled, i.e., the energy barrier amounts to a fourth of the reorganization energy (Table II).

In Fig. 1, the electronic coupling between the ethylene monomers H_{if}^{diab} as a function of the intermolecular distance $R_{C\cdots C}$ is presented. In accordance with the physical model,[10] an exponential decay with increasing intermolecular distance is observed. No significant difference between CASSCF and MR-CISD+P can be seen. A direct comparison of the values

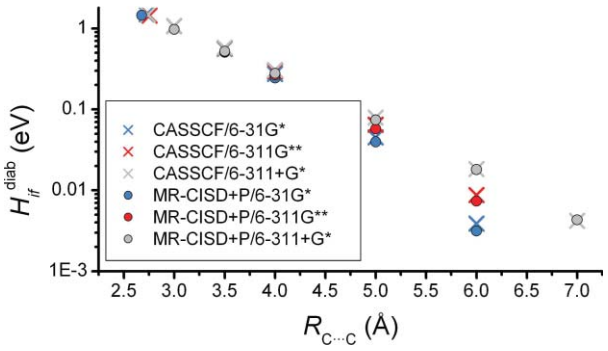

FIG. 1. Dependence of the electronic coupling on the intermolecular distance $R_{C\cdots C}$ in [Et.–Et.]$^+$, computed at the SA(2)-CASSCF(3/4) and MR-CISD+P levels with different basis sets.

(see Supplemental Material S5) shows that there is a small reduction of the gaps by about 10% when dynamical electron correlation is included. This trend has been reported in Ref. 18 as well. At small $R_{C\cdots C}$, basis set effects are negligible. At larger distances, diffuse functions become important showing that an accurate asymptotic behavior of the orbitals is important for describing the interaction.

A two-dimensional plot of the adiabatic potential energy surface of the ground state was computed at the SA(2)-CASSCF(3/4)/6–311+G* level (Fig. 2). It was constructed by first optimizing the symmetric structure at different $R_{C\cdots C}$ values. At each of these structures, the CC bond alternation [ΔR, Eq. (18)] was scanned keeping the remaining internal coordinates fixed. It is expected that $R_{C\cdots C}$ will mainly affect the coupling H_{if}^{diab} [i.e., a modulation between Scheme 1(a) and 1(b)], whereas ΔR should affect the diagonal elements H_{ii}^{diab} and H_{ff}^{diab}. At small $R_{C\cdots C}$ values, a strong coupling behavior is observed in Fig. 2. In this area, the symmetric geometry (ΔR = 0) is stable with respect to changes in ΔR. At $R_{C\cdots C}$ = 2.74 Å, a pronounced symmetric minimum is located which is stabilized by 1.06 eV relative to the noninteracting system. The switch to weak coupling occurs at about $R_{C\cdots C}$ = 4.5 Å. At larger intermolecular separations, the symmetric geometry becomes unstable and two equivalent asymmetric minima are present.

A cut of this surface at $R_{C\cdots C}$ = 5.0 Å is presented in Fig. 3 (only the symmetry unique part, $\Delta R \geq 0$ is shown). In Fig. 3(a), the energies (relative to the noninteracting system) are presented. The adiabatic ground state energy surface is very flat in the neighborhood of the symmetric geometry with a shallow minimum of only 0.003 eV. Diabatic energies were computed according to Eqs. (5) and (7) with the mixing angle η taken from Eq. (6). At the symmetric geometry, one obtains $H_{ii}^{diab} = H_{ff}^{diab}$ (cf. Scheme 1) but through a change in ΔR, this degeneracy is lifted. The lower energy state forms a minimum with a well depth of 0.053 eV at ΔR = 0.06 Å. The gap at this geometry is 0.204 eV. It represents the reorganization energy between the diabatic states. The FCD is plotted in Fig. 3(b). At ΔR = 0, the wave function is delocalized for symmetry reasons and the FCD is zero accordingly. With increasing asymmetry there is a gradual localization of the charge. An FCD of 0.75 is reached at about ΔR = 0.055 Å. In the ground state, the positive charge is localized on the ethylene molecule with the longer CC bond. The excited state shows the same degree of localization with the positive charge

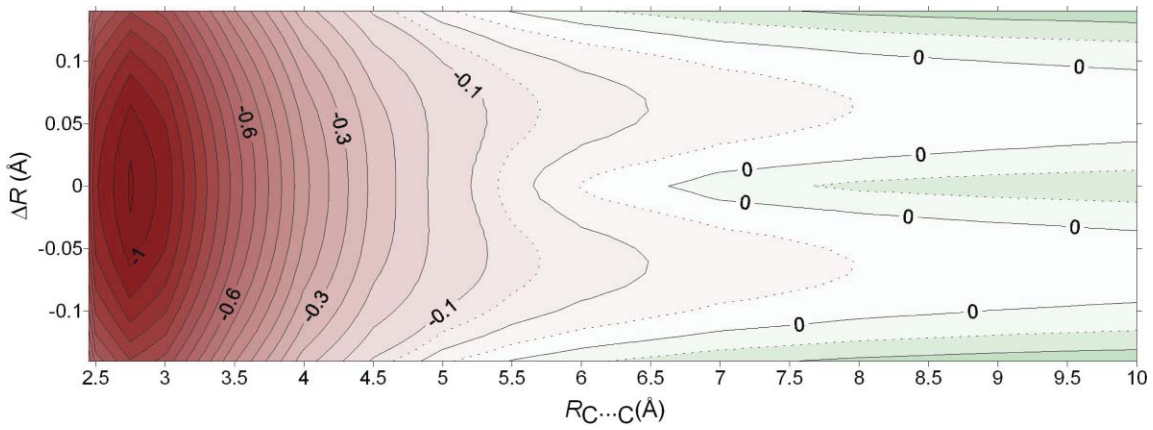

FIG. 2. Doublet ground state potential energy surface of $[Et.–Et.]^+$ (eV) with respect to intermolecular distance $R_{C\cdots C}$ and bond alternation ΔR.

located on the other ethylene molecule. In Fig. 3(c), the component of the nonadiabatic coupling vector along the bond alternation ΔR is shown. The maximum coupling of 11.7 $Å^{-1}$ occurs at $\Delta R = 0$. It gradually decreases as the wave function becomes localized. At 0.05 Å, which is close to the energy minimum, the coupling has decreased to half the maximum value. This means that there still exists quite appreciable coupling throughout the whole region of interest in ΔR. In the two-state model, the coupling should be obtainable from the FCD [Eq. (8) with η derived from Eq. (6)]. This curve is plotted in Fig. 3(c). Very good agreement of the model curve with the directly computed coupling is obtained. It is interesting to compare these plots to the equivalent plots at the larger separation $R_{C\cdots C} = 7.0$ Å (Fig. 4). The general shape is very similar but several features are significantly altered due to the weaker coupling. There is almost no energy splitting and the adiabatic state energies are very close to the charge-localized ones [Fig. 4(a)]. Localization occurs much quicker with displacement in ΔR: an FCD value of 0.75 is already reached at $\Delta R = 0.003$ Å [Fig. 4(b)]. Another striking feature is the nonadiabatic coupling [Fig. 4(c)], which has a much more pronounced peak. The maximum at $\Delta R = 0$ is 227 $Å^{-1}$. A decrease to half of this value occurs already at about $\Delta R = 0.0025$ Å.

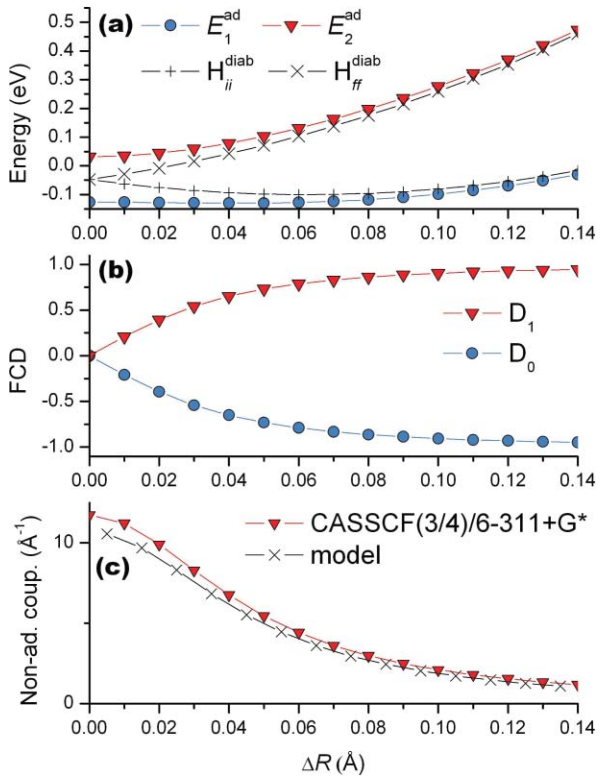

FIG. 3. Adiabatic and diabatic SA-CASSCF energies relative to the noninteracting system, fragment charge differences (FCDs), and nonadiabatic couplings projected on ΔR [analytical and according to the model of Eq. (8) in the text] of $[Et.–Et.]^+$ for an intermolecular distance of $R_{C\cdots C} = 5.0$ Å.

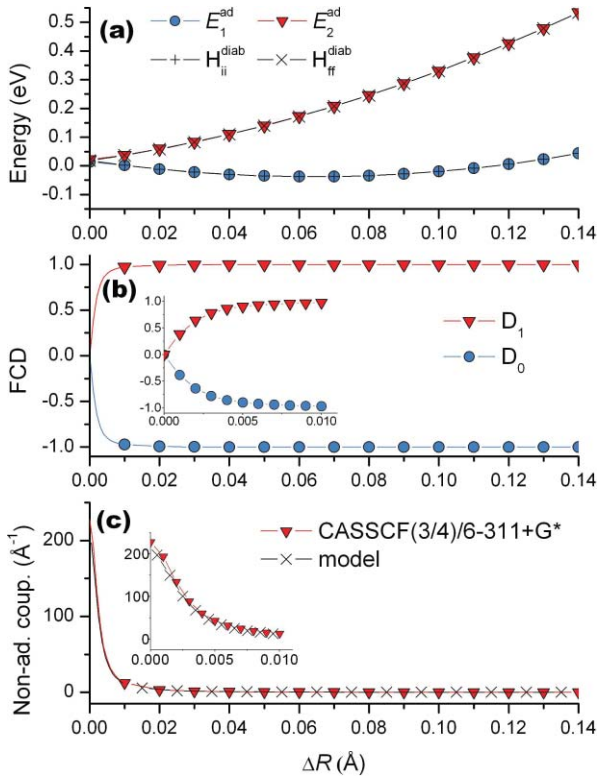

FIG. 4. Adiabatic and diabatic SA-CASSCF energies relative to the noninteracting system, FCDs, and nonadiabatic couplings projected on ΔR [analytical and according to the model of Eq. (8)] of $[Et.–Et.]^+$ for an intermolecular distance of $R_{C\cdots C} = 7.0$ Å.

TABLE III. Relative energies, bridge charges, and character of the first six doublet electronic states of the [Et.–FA–Et.]$^+$ complex considering ionizations out of the π and π^* orbitals.

SA(6)-CASSCF(5/6)				MR-CISD(5/6)+P			
Symm.	Energy (eV)	Ch. on FA	Character	Symm.	Energy (eV)	Ch. on FA	Character
$1\,^2B_1$	0	0.013	$(\pi^-)^1$	$1\,^2B_1$	0	0.013	$(\pi^-)^1$
$1\,^2A_1$	0.087	−0.004	$(\pi^+)^1$	$1\,^2A_1$	0.075	−0.004	$(\pi^+)^1$
$2\,^2B_1$	3.887	0.000	mult.-ref.	$2\,^2B_1$	4.100	0.585	mult.-ref.
$2\,^2A_1$	3.920	0.004	mult.-ref.	$3\,^2B_1$	4.124	0.314	mult.-ref.
$3\,^2B_1$	4.165	0.864	$(\pi^{FA})^1$	$2\,^2A_1$	4.243	0.003	mult.-ref.
$3\,^2A_1$	6.094	0.005	mult.-ref.	$3\,^2A_1$	6.435	0.000	mult.-ref.

In the [Et.–FA–Et.]$^+$ system it is of special interest in which way the bridging formaldehyde is involved in the charge transport. For that reason, the π and π^* orbitals of FA were included in the calculation to estimate their participation in the charge transfer process. CASSCF(5/6) computations were performed which included five electrons in the π and π^* orbitals of each of the three molecules. The first six electronic states were analyzed at the symmetric geometry, i.e., the TS structure of the charge transfer reaction (Table III). MR-CISD+P calculations were performed as well. At the CASSCF level, the first two states are formed by removing an electron from the bonding and antibonding linear combinations of the ethylene π orbitals, respectively. They are separated by a gap of 0.087 eV, i.e., $H_{if}^{\text{diab}} = 0.043\,eV$. This is somewhat larger than the value presented in Table II where only two states were considered in the averaging procedure. Two more states, which are also close in energy, follow at about 4 eV. They have a multireference character where the hole is mainly localized in the ethylene π and π^* orbitals. Ionization of the FA molecule, a $(\pi^{FA})^1$ configuration, corresponds to the fifth state of the system with a relative energy of 4.165 eV. A sixth state with multireference character follows at 6.094 eV. Except for the $(\pi^{FA})^1$ state there is only negligible charge on the bridging molecule. The MR-CISD+P results are quite similar. The couplings are again somewhat reduced (cf. S5 of the Supplemental Material). Both CASSCF and MR-CI calculations agree that no charge on formaldehyde appears up to 4 eV above the ground state. This confirms the picture of an inactive bridge. Rather than playing an active role in the process, the formaldehyde molecule is apparently only involved through reducing the tunneling potential as compared to the vacuum.

B. Dynamics

To simulate the dynamics of the charge-transfer processes, 50 surface-hopping trajectories of 1 ps duration were computed for [Et.–Et.]$^+$ at a separation of $R_{C\ldots C} = 5.0$ Å and for [Et.–FA–Et.]$^+$ at $R_{C\ldots C} = 7.0$ Å. Through restrains on the intermolecular degrees of freedom as described in the Computational Details an almost ideal face-to-face configuration was maintained through the whole course of the dynamics. A sample 300 fs section of the dynamics of [Et.–Et.]$^+$ is shown in Fig. 5. In Fig. 5(a), the energy gap between the two

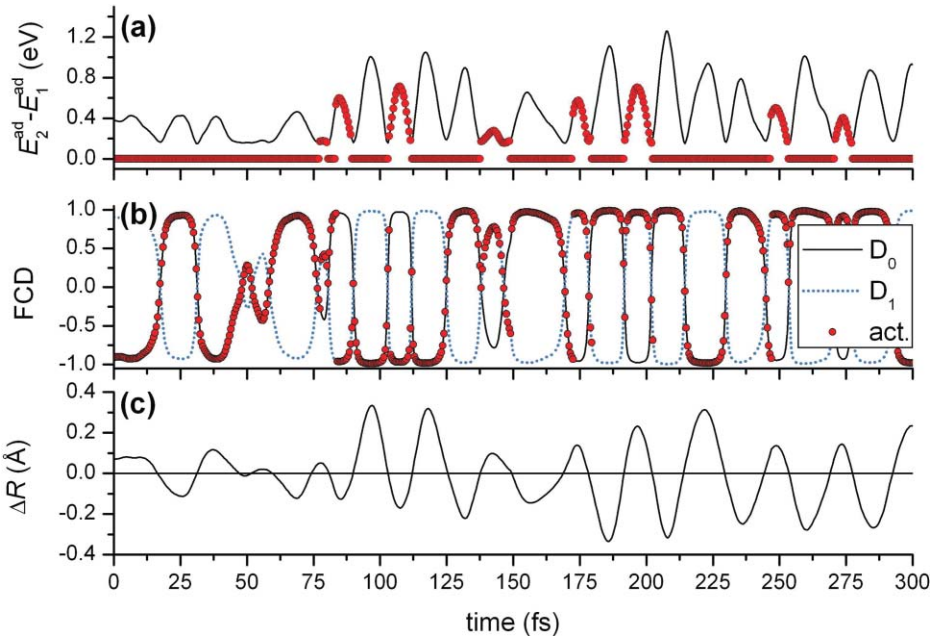

FIG. 5. Energy gap [(a), red circles on the upper line indicate that the system is in the excited state], fragment charge difference (FCD) (b), and CC bond alternation (c) plotted against time for a [Et.–Et.]$^+$ trajectory with $R_{C\ldots C} = 5.0$ Å.

states is plotted. Circles on the upper line are used to indicate that the system is in the excited state. A large gap indicates that the structure is close to a minimum. A reduction in the gap corresponds to approaching the crossing region. It is noted that the gap never goes to zero. This can be understood from the fact that, as mentioned earlier, the diabatic coupling (H_{if}^{diab}) remains fairly constant with restrained intermolecular degrees of freedom. Therefore, an intersection cannot be reached. The gap remains above 0.1 eV for more than 99% of the time in all trajectories (cf. $2H_{if}^{\text{diab}} = 0.158$ eV at the equilibrium geometry, Table II). In Fig. 5(b), the evolution of the FCD against time for the D_0 and D_1 states is presented. The current state of the dynamics is marked with circles. In Fig. 5(c), the time behavior of the CC bond alternation ΔR is shown. This dynamics is now analyzed in terms of the processes defined in Sec. II. A *TS passage* corresponds to a crossing between the FCD curves in Fig. 5(b) (cf. Scheme 3). This happens 20 times in the presented section (18.5, 32.5, 60.5, 91.0, 103.5, 112.5, 126.0, 139.5, 148.5, 170.5, 179.0, 192.5, 202.5, 215.0, 230.5, 245.5, 254.0, 271.0, 278.0, and 293.0 fs). A *TS passage* is usually accompanied also by a sign change of ΔR as shown in Fig. 5(c). However, there is no strict correspondence between these two types of events, as several internal coordinates play a role. In particular, the torsion around the CC bond was seen strongly affecting the relative energetics. This can be understood by the fact that the force constant for this motion in ethylene is strongly altered when removing an electron. The vibrational frequency of this mode changes from 1085 cm^{-1} in the neutral ethylene molecule to 482 cm^{-1} in the cation. In the completely adiabatic case, every *TS passage* would lead to a transfer of charge, i.e., an *active CT* [Scheme 3(a)]. As Scheme 3(b) shows, nonadiabatic coupling between electronic and nuclear motion may inhibit this transfer and lead to a diabatic trapping event. In the plot shown, this type of event occurs, e.g., between 100 and 115 fs where the active state FCD always remains negative even though 2 *TS passages* (103.5 and 112.5 fs) occur. Because of this trapping, only eight *active CTs* (18.5, 32.5, 60.5, 84.0, 126.0, 215.0, 230.5, and 293.5 fs) occur in the section shown. The events of macroscopic interest should start and end in the ground state. In the part shown in Fig. 5, there are 14 *TS global* events (starting at 18.5, 32.5, 60.5, 91.0, 103.5, 126.0, 139.5, 170.5, 192.5, 215.0, 230.5, 245.5, 271.0, and 293.5 fs). Eight r*eal CTs* occur (18.5, 32.5, 60.5, 91.0, 126.0, 215.0, 230.5, and 293.5 fs). From these events κ_{el} and P_{12} were computed according to Eqs. (16) and (17). The averaging was performed for all trajectories, giving statistics over 2559 *TS passages*. The results are presented in Table IV. Approximate results according to Eq. (14) are shown as well using plausible parameter values as follows: H_{if}^{diab} and λ were taken from Table II; $\nu = 1600$ cm^{-1} (as a typical C=C stretch) was chosen; for the effective temperature half the zero-point energy (kinetic energy according to virial theorem) of the C=C vibration was substituted, i.e., $kT = h\nu/4$. Table IV shows that the resulting P_{12} is somewhat larger than the one computed from the dynamics. Very good agreement between the observed value of κ_{el} and the value predicted by Eq. (15) is observed. The overall rate of electron transfer in this complex was 18.7 ps^{-1}.

TABLE IV. Kinetic properties for dynamics of $[\text{Et.–Et.}]^+$ with intermolecular distance $R_{\text{C}\ldots\text{C}} = 5.0$ Å and $[\text{Et.–FA–Et.}]^+$ with $R_{\text{C}\ldots\text{C}} = 7.0$ Å.

	$[\text{Et.–Et.}]^+$		$[\text{Et.–FA–Et.}]^+$	
	Simulation	Eq. (14)	Simulation	Eq. (14)
P_{12}	0.517	0.804	0.287	0.308
$2P_{12}/(1+P_{12})$	0.682	0.891	0.446	0.471
κ_{el}	0.671		0.401	

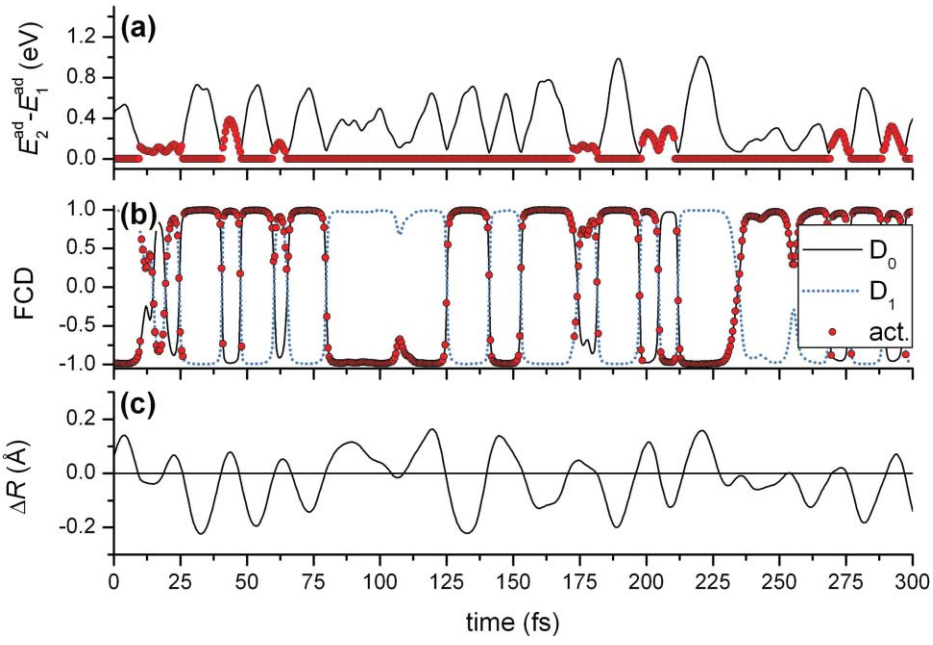

FIG. 6. Energy gap [(a), red dots on the upper line indicate that the system is in the excited state], fragment charge difference (FCD) (b), and CC bond alternation (c) plotted against time for a $[\text{Et.–FA–Et.}]^+$ trajectory with $R_{\text{C}\ldots\text{C}} = 7.0$ Å.

In Fig. 6, the analogous plot for the dynamics of the [Et.–FA–Et.]$^+$ complex is shown. The appearance is quite similar to that of the previous case because the coupling H_{if}^{diab} and reorganization energy λ have comparable values (cf. Table II). The dynamics starts with a *TS global* event, which may be identified as the process shown in Scheme 3(c): there are three *TS passages* (15.5, 20.5, and 25.0 fs), one *active CT* (20.5 fs), and in total a net transfer of charge (a *real CT*). This is followed by two diabatic trapping events [41.0–48.0 fs and 61.0–66.0 fs, cf. Scheme 3(b)] and an adiabatic transfer [80.5 fs, Scheme 3(a)]. The net charge on FA was never more than 0.004*e*. This shows again the picture of an inactive bridge, comparable to the static analysis presented earlier (cf. Table III). In relation to Refs. 4 and 5, we may conclude that a coherent superexchange mechanism without involvement of the bridge takes place here. The charge transfer parameters for this situation are shown in Table IV. The agreement between the static and dynamic descriptions is satisfactory. In particular, the trend between the two complexes is correctly reproduced, i.e., that the charge transfer probability in the second complex is somewhat lower than in the first one. The directly determined value of κ_{el} is slightly smaller than that predicted by Eq. (15). In total, an electron transfer rate of 10.6 ps^{-1} was obtained.

Dynamics calculations with an intermolecular distance of $R_{\text{C}\cdots\text{C}} = 3.0$ Å were performed as well. This case represents a strong coupling situation and purely adiabatic dynamics in the ground state was obtained. The gap was constant at about 2 eV. The hole was always quite delocalized, the absolute value of the FCD never exceeded 0.5. The corresponding graphics is presented in Supplemental Material (S6). The weak coupling case of $R_{\text{C}\cdots\text{C}} = 7.0$ Å, with a theoretical transition probability of about 99.5% per *TS crossing* [Eq. (14)], was examined as well. Because of the highly peaked nonadiabatic coupling [cf. Fig. 4(c)] a very short time-step of well below 0.1 fs would be needed to accurately sample this in the standard formalism. To overcome this problem, surface-hopping based on a locally diabatic representation of the wave function[45] is being implemented into NEWTON-X to allow for efficient accurate sampling of these kinds of processes.

V. CONCLUSIONS

Semiclassical dynamics simulations of charge transfer based on *ab initio* multireference electronic structure methods have been performed for the stacked ethylene dimer radical cation system with insertion of up to three formaldehyde molecules, with the goal of obtaining detailed understanding of the different transfer mechanisms. Computations at the CASSCF and MR-CISD levels allowed for an accurate description of the radical cationic systems including explicit calculation of nonadiabatic coupling between different electronic states. The dynamics of the electron transfer was computed at the level of semiclassical surface hopping with consideration of all nuclear degrees of freedom. Analysis of these simulations and comparison to idealized models, in particular the fragment charge difference (FCD) method, gave interesting insight into the different processes.

The electronic coupling strength within the ethylene dimer radical cation was modulated through the intermolecular distance and the on-site energies through CC bond alternation. Potential energy curves were analyzed in terms of charge delocalization and special focus was given to the nonadiabatic couplings. The CASSCF approach already gave reliable results. Inclusion of dynamic electron correlation through MR-CISD+P slightly reduced electronic couplings (by about 10%) and had a somewhat larger effect on reorganization energies. In the strong coupling region at an intermolecular distance of $R_{\text{C}\cdots\text{C}} = 3.0$ Å, a conventional adiabatic dynamics occurred in a potential characterized by one energy minimum. In the intermediate coupling region, i.e., [Et.–Et.]$^+$ at $R_{\text{C}\cdots\text{C}} = 5.0$ Å and [Et.–FA–Et.]$^+$ at $R_{\text{C}\cdots\text{C}} = 7.0$ Å, interesting complex higher order charge transfers and diabatic trapping situations were observed. These have been analyzed in terms of idealized model processes (Scheme 3). The results were compared to the electronic transmission factor of the Marcus–Levich–Hush theory. In particular, satisfactory agreement and similar trends concerning the dependence of the charge-transfer probability on the intermolecular distance was found between the two methods. Moreover, the simulations of the [Et.–FA–Et.]$^+$ complex showed that FA acts as an inactive bridge molecule there.

The present calculations are intended to initiate general approaches for investigating full nonadiabatic simulations of the dynamics of electronic defects. The currently used direct multireference *ab initio* procedures are restricted to a molecular size comparable to two or three stacked DNA bases. Additionally, quantum mechanics/molecular mechanics (QM/MM) methods[46] may be used to provide a realistic description of environmental effects. Such calculations are intended to serve as benchmarks for subsequent applications to larger systems using simpler, but more cost-effective methods, also allowing significantly longer simulation times.

ACKNOWLEDGMENTS

This work has been supported by the Austrian Science Fund within the framework of the Special Research Programs F16 (Advanced Light Sources) and F41 (ViCoM) and Project P18411-N19. FP is a recipient of a DOC fellowship of the Austrian Academy of Sciences. Computer time at the Vienna Scientific Cluster (project nos. 70019 and 70151) is gratefully acknowledged.

[1] D. B. Hall, R. E. Holmlin, and J. K. Barton, Nature **382**(6593), 731 (1996).
[2] R. G. Endres, D. L. Cox, and R. R. P. Singh, Rev. Mod. Phys. **76**(1), 195 (2004).
[3] F. Garnier, G. Horowitz, X. Z. Peng, and D. Fichou, Synth. Met. **45**(2), 163 (1991); H. E. Katz, A. J. Lovinger, J. Johnson, C. Kloc, T. Siegrist, W. Li, Y. Y. Lin, and A. Dodabalapur, Nature **404**(6777), 478 (2000).
[4] E. Hatcher, A. Balaeff, S. Keinan, R. Venkatramani, and D. N. Beratan, J. Am. Chem. Soc. **130**(35), 11752 (2008).
[5] J. Jortner, M. Bixon, T. Langenbacher, and M. E. Michel-Beyerle, Proc. Natl. Acad. Sci. USA **95**(22), 12759 (1998); B. Giese, J. Amaudrut, A. K. Kohler, M. Spormann, and S. Wessely, Nature **412**(6844), 318 (2001).
[6] N. S. Hush, Trans. Faraday Soc. **57**(4), 557 (1961).
[7] J. Jortner, J. Chem. Phys. **64**(12), 4860 (1976).
[8] B. S. Brunschwig, J. Logan, M. D. Newton, and N. Sutin, J. Am. Chem. Soc. **102**(18), 5798 (1980).
[9] R. A. Marcus, Angewandte Chemie—International Edition in English **32**(8), 1111 (1993).

[10]P. F. Barbara, T. J. Meyer, and M. A. Ratner, J. Phys. Chem. **100** (31), 13148 (1996).
[11]T. Van Voorhis, T. Kowalczyk, B. Kaduk, L. P. Wang, C. L. Cheng, and Q. Wu, Annu. Rev. Phys. Chem. **61**, 149 (2010).
[12]G. A. Jones, B. K. Carpenter, and M. N. Paddon-Row, J. Am. Chem. Soc. **120**(22), 5499 (1998).
[13]L. Blancafort, F. Jolibois, M. Olivucci, and M. A. Robb, J. Am. Chem. Soc. **123**(4), 722 (2001).
[14]A. A. Voityuk and N. Rosch, J. Chem. Phys. **117**(12), 5607 (2002).
[15]T. Kubar, P. B. Woiczikowski, G. Cuniberti, and M. Elstner, J. Phys. Chem. B **112**(26), 7937 (2008).
[16]C. P. Hsu, Acc. Chem. Res. **42**(4), 509 (2009).
[17]A. de la Lande and D. R. Salahub, J. Mol. Struct.: THEOCHEM **943**(1–3), 115 (2010).
[18]L. Blancafort and A. A. Voityuk, J. Phys. Chem. A **110**(20), 6426 (2006).
[19]Y. J. Ye, R. S. Chen, A. Martinez, P. Otto, and J. Ladik, Solid State Commun. **112**(3), 139 (1999).
[20]G. A. Worth, P. Hunt, and M. A. Robb, J. Phy. Chem. A **107** (5), 621 (2003); B. G. Levine and T. J. Martinez, Ann. Rev. Phys. Chem. **58**, 613 (2007); M. Barbatti, M. Ruckenbauer, J. J. Szymczak, A. J. A. Aquino, and H. Lischka, Phys. Chem. Chem. Phys. **10**(4), 482 (2008); M. Barbatti, B. Sellner, A. J. A. Aquino, and H. Lischka, in *Radiation Induced Molecular Phenomena in Nucleic Acid*, edited by M. K. A. L. Shukla, J. (Springer Science + Business Media B.V., 2008).
[21]E. Cauet and J. Lievin, J. Phys. Chem. A **113**(36), 9881 (2009).
[22]L. Blancafort, P. Hunt, and M. A. Robb, J. Am. Chem. Soc. **127**(10), 3391 (2005).
[23]J. C. Tully, J. Chem. Phys. **93**(2), 1061 (1990); S. Hammes-Schiffer and J. C. Tully, J. Chem. Phys. **101**(6), 4657 (1994).
[24]M. Barbatti, R. Shepard, and H. Lischka, in *Conical Intersections: Theory, Computation and Experiment*, edited by W. Domcke, D. R. Yarkony, and H. Köppel (World Scientific, Singapore, 2010), Vol. 17.
[25]J. E. Subotnik, R. J. Cave, R. P. Steele, and N. Shenvi, J. Chem. Phys. **130**, 234102 (2009).
[26]M. D. Newton, Chem. Rev. **91**(5), 767 (1991).
[27]H. Koppel, W. Domcke, and L. S. Cederbaum, Adv. Chem. Phys. **57**, 59 (1984).
[28]L. Landau, Phys. Z. Sowjetunion **2**, 46 (1932).
[29]C. Zener, Proc. R. Soc. London **137**(833), 696 (1932).
[30]J. M. Saveant, J. Phys. Chem. B **106**(36), 9387 (2002).
[31]P. G. Szalay, A. Karpfen, and H. Lischka, Chem. Phys. **130**(1–3), 219 (1989); P. G. Szalay, A. G. Csaszar, G. Fogarasi, A. Karpfen, and H. Lischka, J. Chem. Phys. **93**(2), 1246 (1990); M. Barbatti, J. Paier, and H. Lischka, J. Chem. Phys. **121**(23), 11614 (2004).
[32]P. J. Bruna, S. D. Peyerimhoff, and R. J. Buenker, Chem. Phys. Lett. **72**(2), 278 (1980).
[33]R. Shepard, in *Modern Electronic Structure Theory*, edited by D. R. Yarkony (World Scientific, Singapore, 1995), Vol. 1, p. 345.
[34]J. A. Pople, R. Seeger, and R. Krishnan, Int. J. Quantum Chem. S**11**, 149 (1977).
[35]P. C. Harihara and J. A. Pople, Theoretica Chimica Acta **28**(3), 213 (1973).
[36]R. Krishnan, J. S. Binkley, R. Seeger, and J. A. Pople, J. Chem. Phys. **72**(1), 650 (1980).
[37]H. Lischka, R. Shepard, I. Shavitt, R. M. Pitzer, M. Dallos, T. Mueller, P. G. Szalay, F. B. Brown, R. Ahlrichs, H. J. Boehm, A. Chang, D. C. Comeau, R. Gdanitz, H. Dachsel, C. Ehrhardt, M. Ernzerhof, P. Hoechtl, S. Irle, G. Kedziora, T. Kovar, V. Parasuk, M. J. M. Pepper, P. Scharf, H. Schiffer, M. Schindler, M. Schueler, M. Seth, E. A. Stahlberg, J.-G. Zhao, S. Yabushita, Z. Zhang, M. Barbatti, S. Matsika, M. Schuurmann, D. R. Yarkony, S. R. Brozell, E. V. Beck, J.-P. Blaudeau, M. Ruckenbauer, B. Sellner, F. Plasser, and J. J. Szymczak, COLUMBUS, an ab initio electronic structure program, Release 5.9.1, www.univie.ac.at/columbus (2006).
[38]T. Helgaker, H. J. A. Jensen, P. Jørgensen, J. Olsen, K. Ruud, H. Ågren, T. Andersen, K. L. Bak, V. Bakken, O. Christiansen, P. Dahle, E. K. Dalskov, T. Enevoldsen, H. Heiberg, H. Hettema, D. Jonsson, S. Kirpekar, R. Kobayashi, H. Koch, K. V. Mikkelsen, P. Norman, M. J. Packer, T. Saue, P. R. Taylor, and O. Vahtras, DALTON, an *ab initio* electronic structure program, Release 1.0 (1997).
[39]M. Barbatti, G. Granucci, M. Persico, M. Ruckenbauer, M. Vazdar, M. Eckert-Maksic, and H. Lischka, J. Photochem. Photobiol., A **190**(2–3), 228 (2007).
[40]M. Barbatti, G. Granucci, M. Ruckenbauer, M. Persico, and H. Lischka, NEWTON-X: A package for Newtonian dynamics close to the crossing seam, version 1.1.4b, (2007).
[41]G. Granucci and M. Persico, J. Chem. Phys. **126**(13), 134114 (2007).
[42]R. Shepard, H. Lischka, P. G. Szalay, T. Kovar, and M. Ernzerhof, J. Chem. Phys. **96**(3), 2085 (1992); H. Lischka, M. Dallos, and R. Shepard, Mol. Phys. **100**(11), 1647 (2002); M. Dallos, H. Lischka, R. Shepard, D. R. Yarkony, and P. G. Szalay, J. Chem. Phys. **120**(16), 7330 (2004); H. Lischka, M. Dallos, P. G. Szalay, D. R. Yarkony, and R. Shepard, J. Chem. Phys. **120**(16), 7322 (2004).
[43]W. J. Hehre, R Ditchfield, and J. A. Pople, J. Chem. Phys. **56**(5), 2257 (1972).
[44]See supplementary material at http://dx.doi.org/10.1063/1.3526697 for geometries and total energies of the complexes considered, a collection of electronic couplings at different levels of theory, and a dynamics analysis of [Et.-Et.]$^+$ with 3.0 A intermolecular distance.
[45]G. Granucci, M. Persico, and A. Toniolo, J. Chem. Phys. **114**(24), 10608 (2001).
[46]D. Bakowies and W. Thiel, J. Phys. Chem. **100**(25), 10580 (1996); M. Ruckenbauer, M. Barbatti, T. Muller, and H. Lischka, J. Phys. Chem. A **114**(25), 6757 (2010).